CHINESE OPTICS LETTERS

Vol. 21, No. 7 | July 2023

Self-focusing of partially coherent beams based on complex screen and split-step Fourier transform methods

Fanglun Yang (杨方伦)[1,2,3], Guowen Zhang (张国文)[2,3,4*], Xiaoqi Zhang (张笑琪)[2,3], Yanli Zhang (张艳丽)[2,3], Ruifeng Wang (王瑞峰)[2,3,4], and Jianqiang Zhu (朱健强)[2,3**]

[1] School of Physical Sciences, University of Science and Technology of China, Hefei 230026, China

[2] Key Laboratory of High Power Laser and Physics, Shanghai Institute of Optics and Fine Mechanics, Chinese Academy of Sciences, Shanghai 201800, China

[3] National Laboratory on High Power Laser and Physics, Shanghai Institute of Optics and Fine Mechanics, Chinese Academy of Sciences, Shanghai 201800, China

[4] University of Chinese Academy of Sciences, Beijing 100049, China

*Corresponding author: guowenzhang@siom.ac.cn

**Corresponding author: jqzhu@siom.ac.cn

Received February 14, 2023 | Accepted April 14, 2023 | Posted Online July 10, 2023

The self-focusing phenomenon of partially coherent beams (PCBs) was simulated using the complex screen method combined with the split-step Fourier method to solve the nonlinear Schrödinger equation. Considering the propagation of Gaussian Schell-model beams in a nonlinear medium as an example, the suppression effects of intensity, propagation distance, and spatial coherence on small-scale self-focusing were demonstrated. Simulations of overall and small-scale self-focusing using this method were compared with the existing literature to demonstrate the validity of the method. This method can numerically analyze the degree of self-focusing in PCBs and advance the study of their nonlinearity.

Keywords: partially coherent beams; self-focusing; nonlinearity; complex screen method; Gaussian Schell-model.
DOI: 10.3788/COL202321.071901

1. Introduction

High-power laser drivers play an important role in high-energy, high-density physics, such as inertial confinement fusion, laser plasma physics, and laboratory astrophysics. When a high-power laser propagates in a nonlinear medium, a self-focusing phenomenon occurs owing to nonlinear effects, which is a major factor that limits the laser output power and damages the beam quality. The Bespalov–Talanov (B-T) theory was the first to provide a simple and clear explanation of self-focusing filaments of coherent light[1,2], which was experimentally verified by Bliss in the 1960s[3,4]. Small-scale self-focusing is the main factor leading to the deterioration of beam quality and limits the load of the laser driver[5–7]. Partially coherent beams (PCBs) have been developed as laser drivers because they suppress nonlinear effects and improve the uniformity of the optical field[8–18]. To date, much work has been conducted on the propagation of fully coherent beams in nonlinear media. However, few studies have focused on PCBs[19–21].

In optical coherence theory[22], the calculation of the inevitable four-dimensional integrals during the propagation of PCBs increases the analytical complexity. Coherent modal representation (CMR)[23,24], pseudo-modal representation (PMR)[25], and random modal representation (RMR) were introduced to reduce computational difficulty[26].

RMR primarily refers to the complex screen (CS) method used to construct PCBs, which can flexibly and reliably represent various beam distributions of Schell light sources. The random CS method has great potential for solving the problem of propagating of PCBs in nonlinear media. In 2014, David *et al.* proposed the Gaussian Schell-model (GSM) beam representation using the CS method and demonstrated its effectiveness by comparing it with the GSM constructed by the theoretical method[27]. In 2015, this method was used to flexibly and conveniently simulate PCB fields with various far-field distributions[28]. In 2017, Wang *et al.* used the CS method to calculate and experimentally verify the propagation of partially coherent crescent-like optical beams in free space and turbulent atmosphere[29]. In 2022, Wang *et al.* extended the CS approach to the time-frequency domain of Schell-model beams and simulated the computational Schell-model transport in a nonlinear medium[30] by comparing it with the pulse-by-phase method[31] to verify the correctness of their method. In addition to the CS method, an analytical method for the steady-state self-focusing of the GSM in a nonlinear media was studied by Wang *et al.* in 2019[32] and extended it to the quasi-steady-state case in

2020[33]. This theory yields important propagation characteristics of the GSM in nonlinear media under the approximation that the beams maintain the GSM after passing through it. In 2022, Lu *et al.* studied the self-focusing property of PCBs with nonuniform correlation structures in nonlinear media and demonstrated the feasibility of controlling the self-focusing length by controlling the initial coherence radius[34].

In this study, we propose a method for numerically solving the nonlinear Schrödinger (NLS) equation using the random CS and split-step Fourier methods, which can be used to calculate the self-focusing of PCBs in nonlinear media. To demonstrate the validity of the method, we compare the beam intensity evolution under the overall self-focusing of the GSM in the proposed and analytical formula methods[32] and compare the small-scale self-focusing phenomenon of the GSM and a coherent Gaussian beam in this study. This method allows the numerical analysis of the degree of self-focusing of the Schell-model beams, extends the range of sources for which self-focusing can be calculated, and is important for assessing the load capability of new high-power laser drivers using spatially PCBs.

2. Theoretical Model

2.1. Random CS method

The Schell-model beams are expressed in terms of the cross-spectral density functions $W(\boldsymbol{r}_1,\boldsymbol{r}_2,z)$, which can be expressed as

$$W(\boldsymbol{r}_1,\boldsymbol{r}_2,z)=\langle T(\boldsymbol{r}_1,z)T^*(\boldsymbol{r}_2,z)\rangle=E(\boldsymbol{r}_1)E^*(\boldsymbol{r}_2)\mu(\boldsymbol{r}_1,\boldsymbol{r}_2). \quad (1)$$

In the CS method[26,27], the PCB is represented by an incoherent superposition of spatially random complex fields. The instantaneous scalar field (single realization) $T_n(\boldsymbol{r})$ can be expressed as the product of the coherent electric field $E(\boldsymbol{r})$ and random CS transmittance function $\psi_n(\boldsymbol{r})$,

$$T_n(\boldsymbol{r})=E(\boldsymbol{r})\psi_n(\boldsymbol{r}). \quad (2)$$

Substituting Eq. (2) into Eq. (1), we obtain Eq. (3).

$$W(\boldsymbol{r}_1,\boldsymbol{r}_2,z)=E(\boldsymbol{r}_1)E^*(\boldsymbol{r}_2)\langle\psi_n(\boldsymbol{r}_1)\psi_n^*(\boldsymbol{r}_2)\rangle. \quad (3)$$

According to Refs. [35,36], the coherence function $\mu(\boldsymbol{r}_1,\boldsymbol{r}_2)$ can be expressed as

$$\mu(\boldsymbol{r}_1,\boldsymbol{r}_2)=\int p(\boldsymbol{v})\exp[-i(\boldsymbol{r}_1-\boldsymbol{r}_2)\boldsymbol{v}]\mathrm{d}v, \quad (4)$$

where $p(\boldsymbol{v})$ is a non-negative function.

$$\langle C_n(\boldsymbol{v}_1)C_n^*(\boldsymbol{v}_2)\rangle=\delta(\boldsymbol{v}_1-\boldsymbol{v}_2), \quad (5)$$

where $\delta(\boldsymbol{v}_1-\boldsymbol{v}_2)$ is the Dirac delta function, and $C_n(\boldsymbol{v})$ is a white noise electric field with the properties of Eq. (5). Expressing $\psi_n(\boldsymbol{r})$ in the form of Eq. (6) and substituting Eq. (4), Eq. (5), and Eq. (6) into Eq. (3), we obtain Eq. (1).

$$\psi_n(\boldsymbol{r})=\int\sqrt{p(\boldsymbol{v})}C_n(\boldsymbol{v})\exp(-i2\pi\boldsymbol{r}\cdot\boldsymbol{v})\mathrm{d}\boldsymbol{v}. \quad (6)$$

When the number of complex screens N is sufficiently large, $W(\boldsymbol{r}_1,\boldsymbol{r}_2,z)$ can be expressed as

$$W(\boldsymbol{r}_1,\boldsymbol{r}_2,z)\approx\frac{1}{N}\sum_{n=1}^{N}T_n(\boldsymbol{r}_1)T_n^*(\boldsymbol{r}_2). \quad (7)$$

The cross-spectral density function of the GSM is expressed as

$$W(\boldsymbol{r}_1,\boldsymbol{r}_2,z)=I_0\exp\left(-\frac{\boldsymbol{r}_1^2+\boldsymbol{r}_2^2}{\omega_0^2}\right)\exp\left[-\frac{(\boldsymbol{r}_1-\boldsymbol{r}_2)^2}{2\rho_0^2}\right], \quad (8)$$

where I_0 denotes the initial intensity. Using the CS method to represent the GSM, the coherent electric field, coherence function, and intensity distribution are given by Eqs. (9), (10), and (11), respectively.

$$E(r)=E_0\exp\left(-\frac{\boldsymbol{r}^2}{\omega_0^2}\right), \quad (9)$$

$$\mu(\boldsymbol{r}_1,\boldsymbol{r}_2)=\frac{W(\boldsymbol{r}_1,\boldsymbol{r}_2,z)}{\sqrt{W(\boldsymbol{r}_1,\boldsymbol{r}_1,z)W(\boldsymbol{r}_2,\boldsymbol{r}_2,z)}}=\exp\left[-\frac{(\boldsymbol{r}_1-\boldsymbol{r}_2)^2}{2\rho_0^2}\right], \quad (10)$$

$$I(\boldsymbol{r})=\langle|T(\boldsymbol{r})|^2\rangle\approx\frac{1}{N}\sum_{1}^{N}|T_n(\boldsymbol{r})|^2. \quad (11)$$

2.2. Propagation of PCBs in a nonlinear Kerr medium

Under the steady-state and standard paraxial approximations, the NLS equation for PCBs in nonlinear Kerr medium is

$$\left[2\mathrm{i}k\frac{\partial}{\partial z}+(\nabla_{\perp1}^2-\nabla_{\perp2}^2)\right]W(\boldsymbol{r}_1,\boldsymbol{r}_2,z)+2k^2\frac{n_2[W(\boldsymbol{r}_1,\boldsymbol{r}_1,z)-W(\boldsymbol{r}_2,\boldsymbol{r}_2,z)]}{n_0}W(\boldsymbol{r}_1,\boldsymbol{r}_2,z)=0, \quad (12)$$

where $\nabla_\perp^2=\nabla_x^2+\nabla_y^2$ is the transverse Laplace operator and n_2 is the nonlinear refractive index. Usually the equation has no analytical solution and can be solved numerically by the split-step Fourier method[37]. The key to solving the above equation using the split-step Fourier method is two parts: the diffraction part and the self-focusing effect part.

The diffraction part can be expressed as

$$2\mathrm{i}k\frac{\partial}{\partial z}W(\boldsymbol{r}_1,\boldsymbol{r}_2,z)+(\nabla_{\perp1}^2-\nabla_{\perp2}^2)W(\boldsymbol{r}_1,\boldsymbol{r}_2,z)=0. \quad (13)$$

This equation represents the diffraction transport of the PCBs. The CS method perfectly represents the process and

has been applied to the transport of PCBs in free space under atmospheric turbulence[26,27].

The nonlinear part can be expressed as

$$\frac{\partial}{\partial z}W(\boldsymbol{r}_1,\boldsymbol{r}_2,z)=W(\boldsymbol{r}_1,\boldsymbol{r}_2,z)\times \mathrm{i}k\frac{n_2[W(\boldsymbol{r}_1,\boldsymbol{r}_1,z)-W(\boldsymbol{r}_2,\boldsymbol{r}_2,z)]}{n_0}. \tag{14}$$

For a small Δz, Eq. (14) can be expressed as

$$W(\boldsymbol{r}_1,\boldsymbol{r}_2,z+\Delta z) = W(\boldsymbol{r}_1,\boldsymbol{r}_2,z)\times \exp\left[\mathrm{i}k\frac{n_2[W(\boldsymbol{r}_1,\boldsymbol{r}_1,z)-W(\boldsymbol{r}_2,\boldsymbol{r}_2,z)]}{n_0}\times\Delta z\right]. \tag{15}$$

The CS rule is calculated as follows:

$$\frac{\partial}{\partial z}T_n(\boldsymbol{r},z)=\mathrm{i}k\frac{n_2\langle|T(\boldsymbol{r})|^2\rangle}{n_0}T_n(\boldsymbol{r},z). \tag{16}$$

For a small Δz, Eq. (16) can be expressed as

$$T_n(\boldsymbol{r},z+\Delta z)=\exp\left[\mathrm{i}k\frac{\langle n_2|T(\boldsymbol{r})|^2\rangle}{n_0}\times\Delta z\right]\times T_n(\boldsymbol{r},z). \tag{17}$$

By substituting T_n at $\boldsymbol{r}_1,\boldsymbol{r}_2$ into Eq. (2) according to Eq. (17), we obtain Eq. (15).

In addition, to demonstrate the small-scale self-focusing phenomenon of PCBs, we let the beam first pass through screen $t(x,y)$ of periodic transmittance as a small-scale modulation with the following transmittance before solving the NLS equation[4,38]:

$$t(x,y)=[1+a\times\sin(2\pi f_x x)]^{1/2}, \tag{18}$$

where a and f_x denote the initial modulation depth of the intensity and modulation period, respectively. The degree of self-focusing is characterized by the local modulation degree (M), where $I_{\max}$ and $I_{\min}$ denote the maximum and minimum intensities in the local area, respectively.

$$M=\frac{I_{\max}-I_{\min}}{I_{\max}+I_{\min}}. \tag{19}$$

3. Numerical Results and Analysis

In this section, the above theoretical model is used to simulate the overall and small-scale self-focusing processes of the GSM. The nonlinear medium was neodymium glass, which is now extensively used in high-power laser systems. It has a refractive index (n_0) of 1.54 and a nonlinear refractive index (n_2) of 1.18×10^{-13} esu. The beam radius (w_0) is 4 mm, and $C=w_0/\rho_0$ denotes the ratio of the beam width w_0 to the coherence length ρ_0.

First, we calculated the variation in the maximum intensity for the overall self-focusing of the GSM. Three cases of coherent beams, $C=2$, and $C=3$, with an initial intensity of 0.2 GW/cm^2 and a length of 4.5 m for the nonlinear medium, were assigned.

The evolution of the maximum intensity of each beam under overall self-focusing, as calculated using the analytical formula and CS methods, is shown in Fig. 1. The coherent beam (NSL) is the numerical solution of the NLS equation using a coherent Gaussian beam. AF is the analytical formula in Ref. [32]. CS is the simulation result obtained using the random complex screen method. As shown in Fig. 1, the AF and CS methods fit well in all three cases, proving the reliability of the methods.

Next, the propagation of the coherent Gaussian beam and the GSM in a nonlinear medium at a certain intensity after the perturbation were simulated. The simulation method for the small-scale self-focusing of coherent beams has been well established and proven to be correct. Therefore, we included the simulation of a coherent beam as a reference for comparison with the PCBs. The length of the nonlinear medium was 400 mm. In the transmittance screen function $t(x,y)$, $a=0.1$, and $f_x=11.9$/cm. $C=2$, 5, 10, and 20 were set for the GSM, corresponding to the coherence lengths ρ_0 of 2, 0.8, 0.4, and 0.2 mm, respectively. The w_0 values are all 4 mm. The number of complex screens N is 2000, at which point the coherence function for each case can be better represented.

Figure 2 represents the intensity distribution of each beam with an initial intensity of 2.6 GW/cm^2 after amplitude modulation and propagation through 400-mm Nd glass medium, where Figs. 2(a)–2(e) represent the coherent beam, and $C=2$, 5, 10, and 20, respectively, and Fig. 2(f) represents the one-dimensional distribution of each beam at $y=0$.

Figure 3 shows the parameter variation of each beam on the transmission path for an initial intensity of 2.6 GW/cm^2. Figure 3(a) shows the variation in the degree of modulation on the transmission path, while Fig. 3(b) shows the variation in the maximum intensity on the transmission path. Figures 4 and 5 are similar to Figs. 2 and 3, except that Figs. 4 and 5

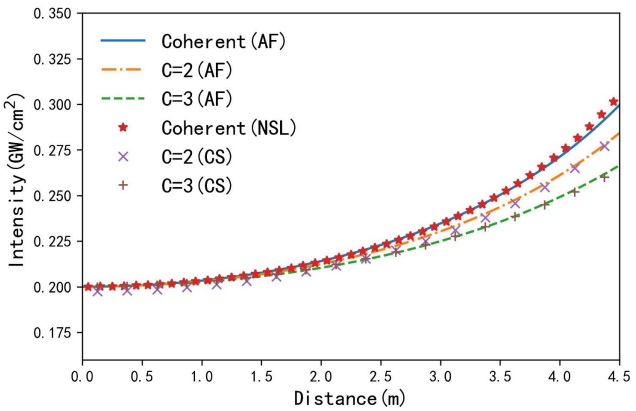

Fig. 1. Comparison of the analytical formula and the CS methods for overall self-focusing.

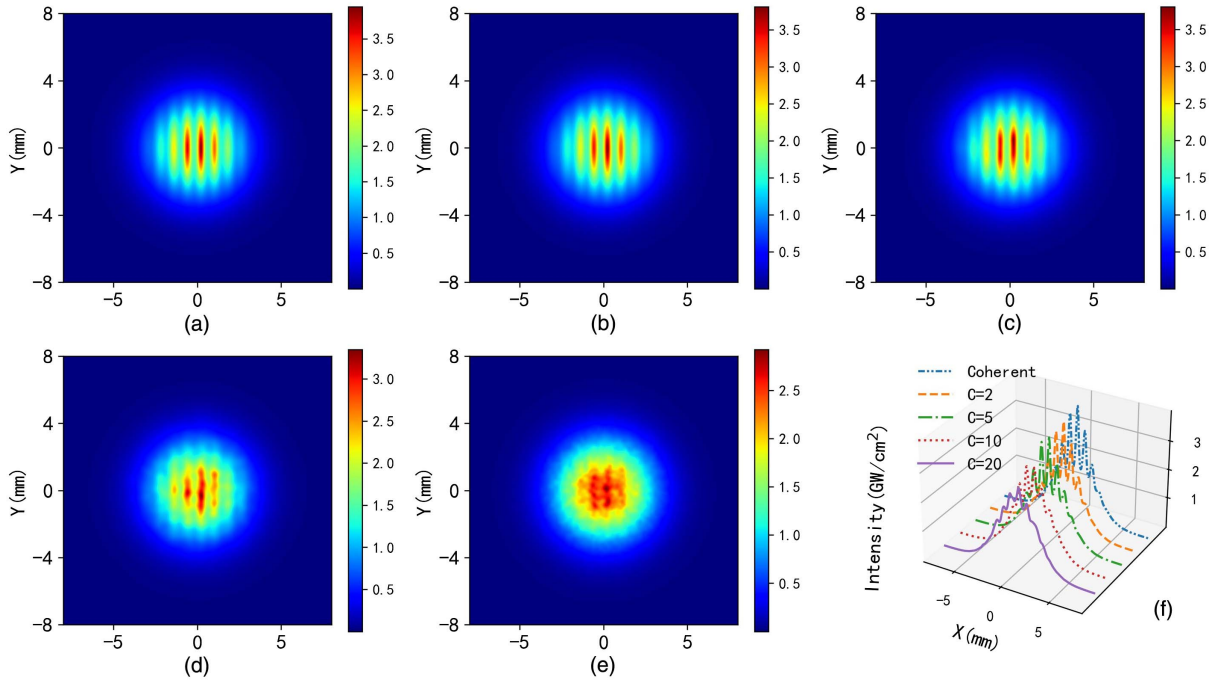

Fig. 2. Beam distribution with the initial intensity of 2.6 GW/cm^2 after 400-mm transmission. (a), (b), (c), (d), and (e) correspond to the coherent beam, and $C = 2$, 5, 10, and 20, respectively. (f) The one-dimensional distribution corresponding to each light field at $y = 0$.

correspond to an initial intensity of 4 GW/cm^2. The coherence shown in Figs. 2–5 is the numerical solution to the NLS equation using a coherent Gaussian beam. In the two cases of the combined initial intensity of 2.6 GW/cm^2 and 4 GW/cm^2, the evolution of the beam distribution, modulation degree, and maximum intensity of $C = 2$ and the coherent beam can coincide more perfectly. This demonstrates the reliability of the method of solving the NLS equation to some extent.

According to Figs. 3 and 5, the modulation degree M and the maximum intensity increase with the diffraction distance when the initial intensity is the same. The change trends of both are essentially the same and are close to exponential growth, which is typical of the small-scale self-focusing effect. This phenomenon is also observed in PCBs. However, the modulation growth trend differs for each coherent GSM length.

Table 1 summarizes the final modulation degree at various coherence and initial intensities. Stronger initial intensities yield higher final modulation degrees. The higher coherence corresponds to the higher final modulation degrees. Therefore, reducing the initial intensity and coherence can slow the growth of the modulation degree and maximum intensity and suppress the self-focusing effect.

At an initial intensity of 4 GW/cm^2, the final modulation degree of 0.19 for the $C = 20$ Gaussian Schell-mode was 73.6% lower than the 0.72 for the coherent beam. This is also significantly lower than those of the other GSMs. When the

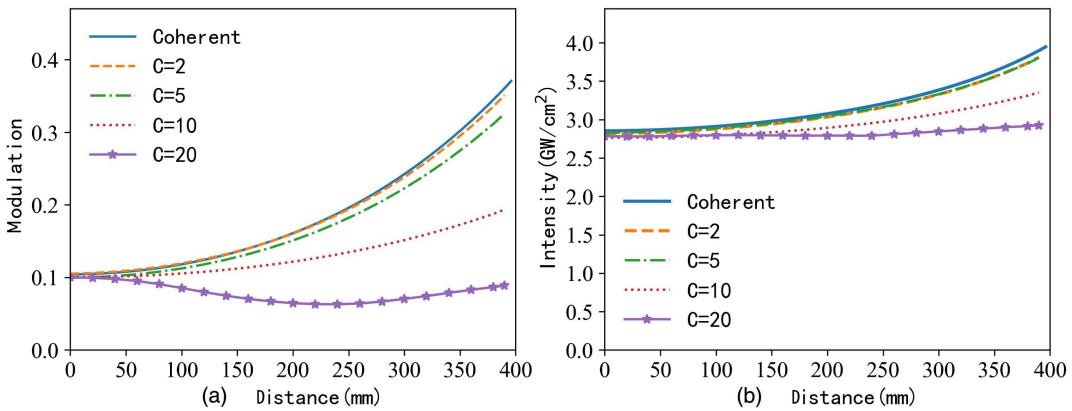

Fig. 3. Variation of the beam in (a) the modulation system and (b) the maximum intensity at an initial intensity of 2.6 GW/cm^2.

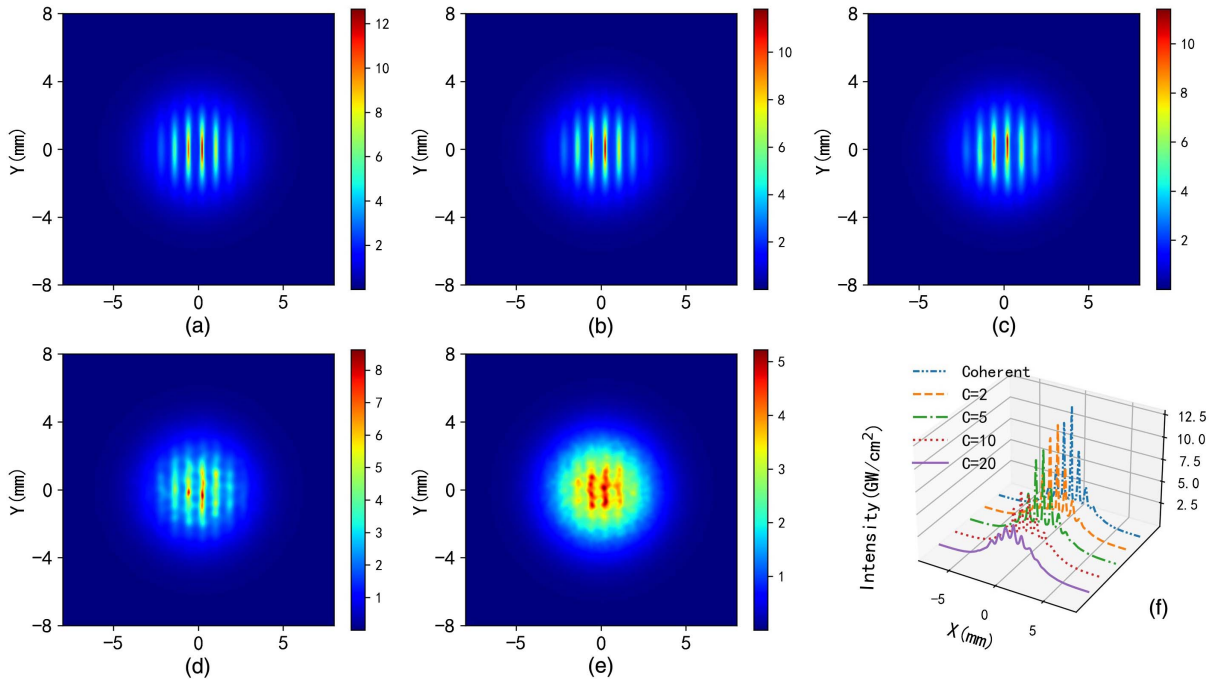

Fig. 4. Beam distribution with the initial intensity of 4 GW/cm^2 after 400-mm transmission. (a), (b), (c), (d), and (e) correspond to the coherent beam, and C = 2, 5, 10, and 20, respectively. (f) The one-dimensional distribution corresponding to each light field at y = 0.

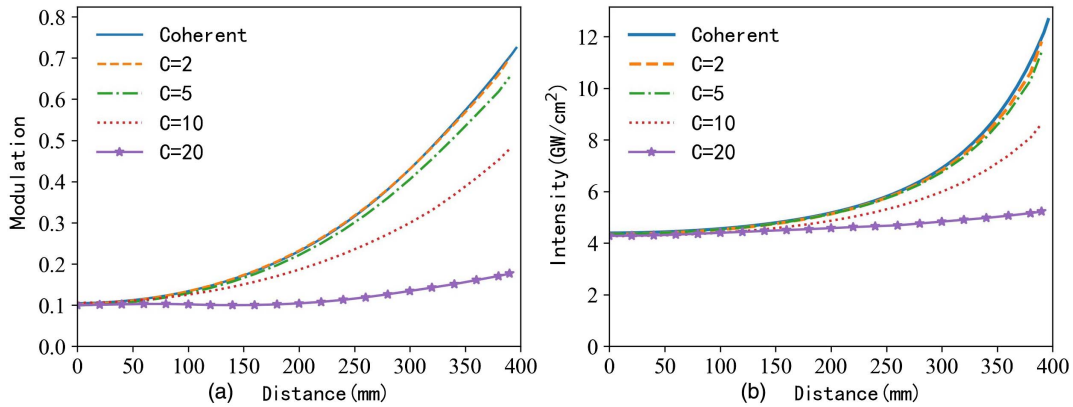

Fig. 5. Variation of the beam in (a) the modulation system and (b) the maximum intensity at an initial intensity of 4 GW/cm^2.

initial intensity is 2.6 GW/cm^2, the modulation degree even decreases from 0.1 to the final 0.09. In this case, the diffraction effect surpasses self-focusing, and small-scale perturbations appear as spatial diffusion.

Table 1. Modulation Degree M after Propagating through 400-mm Nd Glass.

	Coherent	C = 2	C = 5	C = 10	C = 20
2.6 GW/cm^2	0.37	0.35	0.33	0.19	0.09
4 GW/cm^2	0.72	0.70	0.66	0.46	0.19

4. Conclusion

This study presents a method for calculating the transmission of spatially PCBs in a nonlinear media using the CS method combined with the split-step Fourier method, which solves the problem of the transmission of PCBs in a nonlinear Kerr media. The evolution of the overall self-focused maximum intensity of the GSM was compared using the CS and the analytical formula methods, which verified the effectiveness of the method. Simulations of the nonlinear propagation of the GSM with modulation demonstrated the effects of factors such as spatial coherence, intensity, and transmission distance on the modulation degree of self-focusing. The simulation results showed that small-scale self-focusing also occurred in PCBs. However, low

spatial coherence can suppress the degree of self-focusing. When the GSM coherence was high, the small-scale self-focusing behavior was very similar to that of the coherent beam, which laterally reflected the effectiveness of the CS method.

This method facilitates a quantitative analysis of the overall and small-scale self-focusing degree of the Schell-model beams and is expected to establish a theory applicable to the modulation instability of PCBs in nonlinear media, which is of great significance for designing the seed source of high-power PCB laser devices and evaluating the load capacity.

Acknowledgement

This work was supported by the Strategic Priority Research Program of the Chinese Academy of Sciences (Nos. XDA25020203 and 25020301) and the Innovation Fund of the Key Laboratory of the Chinese Academy of Sciences (No. CXJJ- 21S015).

References

1. V. I. Bespalov and V. I. Talanov, "Filamentary structure of light beams in nonlinear liquids," JETP Lett. **3**, 307 (1966).
2. M. M. T. Loy and Y. R. Shen, "Small-scale filaments in liquids and tracks of moving foci," Phys. Rev. Lett. **22**, 994 (1969).
3. A. J. Campillo, S. L. Shapiro, and B. R. Suydam, "Periodic breakup of optical beams due to self-focusing," Appl. Phys. Lett. **23**, 628 (1973).
4. E. S. Bliss, D. R. Speck, J. F. Holzrichter, J. H. Erkkila, and A. J. Glass, "Propagation of a high-intensity laser pulse with small-scale intensity modulation," Appl. Phys. Lett. **25**, 448 (1974).
5. J. A. Fleck, Jr. and C. Layne, "Study of self-focusing damage in a high-power Nd: glass-rod amplifier," Appl. Phys. Lett. **22**, 467 (1973).
6. E. Bliss, J. Hunt, P. Renard, G. Sommargren, and H. Weaver, "Effects of nonlinear propagation on laser focusing properties," IEEE J. Quantum Electron. **12**, 402 (1976).
7. S.-C. Wen and D.-Y. Fan, "Non-paraxial propagation of optical beams in nonlinear self-focusing media," Chin. J. Lasers **28**, 1066 (2001).
8. Y. Kato, K. Mima, N. Miyanaga, S. Arinaga, Y. Kitagawa, M. Nakatsuka, and C. Yamanaka, "Random phasing of high-power lasers for uniform target acceleration and plasma-instability suppression," Phys. Rev. Lett. **53**, 1057 (1984).
9. X. Deng, X. Liang, Z. Chen, W. Yu, and R. Ma, "Uniform illumination of large targets using a lens array," Appl. Opt. **25**, 377 (1986).
10. S. Skupsky, R. W. Short, T. Kessler, R. S. Craxton, S. Letzring, and J. M. Soures, "Improved laser-beam uniformity using the angular dispersion of frequency-modulated light," J. Appl. Phys. **66**, 3456 (1989).
11. N. A. Fleurot, M. L. Andre, P. Estraillier, D. Friart, C. Gouedard, C. Rouyer, J. P. Thebault, G. Thiell, and D. Veron, "Output pulse and energy capabilities of the PHEBUS laser facility," Proc. SPIE **1502**, 230 (1991).
12. H. Nakano, N. Miyanaga, K. Yagi, K. Tsubakimoto, M. Nakatsuka, and S. Nakai, "Partially coherent light generated by using single and multimode optical fibers in a high-power Nd:glass laser system," Appl. Phys. Lett. **63**, 580 (1993).
13. M. Nakatsuka, N. Miyanaga, T. Kanabe, H. Nakano, K. Tsubakimoto, and S. Nakai, "Partially coherent light sources for ICF experiment," Proc. SPIE **1870**, 151 (1993).
14. S. I. Fedotov, L. P. Feoktistov, M. V. Osipov, and A. N. Starodub, "Lasers for ICF with a controllable function of mutual coherence of radiation," J. Russ. Laser Res. **25**, 79 (2004).
15. Y. Gao, L. Ji, X. Zhao, Y. Cui,*et al.*, "High-power, low-coherence laser driver facility," Opt. Lett. **45**, 6839 (2020).
16. A. Shaykin, V. Ginzburg, I. Yakovlev, A. Kochetkov, A. Kuzmin, S. Mironov, I. Shaikin, V. Lozhkarov, A. Prokhorov, and E. Khazanov, "Use of KDP crystal as a Kerr nonlinear medium for compressing PW laser pulses down to 10 fs," High Power Laser Sci. Eng. **9**, e54 (2021).
17. C. Liang, Y. E. Monfared, X. Liu, B. Qi, F. Wang, O. Korotkova, and Y. Cai, "Optimizing illumination's complex coherence state for overcoming Rayleigh's resolution limit," Chin. Opt. Lett. **19**, 052601 (2021).
18. Y. Zhu, Z. Zheng, X. Ge, G. Du, S. Ruan, C. Guo, P. Yan, P. Hua, L. Xia, and Q. Lü, "High-power, ultra-broadband supercontinuum source based upon 1/1.5 μm dual-band pumping," Chin. Opt. Lett. **19**, 041403 (2021).
19. Z. Chen, J. Klinger, and D. N. Christodoulides, "Induced modulation instability of partially spatially incoherent light with varying perturbation periods," Phys. Rev. E Stat Nonlin Soft Matter Phys **66**, 066601 (2002).
20. J. Xu, Z. Liu, K. Pan, and D. Zhao, "Asymmetric rotating array beams with free movement and revolution," Chin. Opt. Lett. **20**, 022602 (2022).
21. M. Soljacic, M. Segev, T. Coskun, D. N. Christodoulides, and A. Vishwanath, "Modulation instability of incoherent beams in noninstantaneous nonlinear media," Phys. Rev. Lett. **84**, 467 (2000).
22. F. Bashore and A. Norcross, *Optical Coherence and Quantum Optics* (Cambridge University Press, 1996).
23. E. Wolf, "New spectral representation of random sources and of the partially coherent fields that they generate," Opt. Commun. **38**, 3 (1981).
24. E. Wolf, "New theory of partial coherence in the space–frequency domain. Part I: spectra and cross spectra of steady-state sources," J. Opt. Soc. Am. **72**, 343 (1982).
25. Y. Gu and G. Gbur, "Scintillation properties of pseudo-Bessel correlated beams in atmospheric turbulence," Proc. SPIE **7924**, 792404 (2011).
26. F. Wang, H. Lv, Y. Chen, Y. Cai, and O. Korotkova, "Three modal decompositions of Gaussian Schell-model sources: comparative analysis," Opt. Express **29**, 29676 (2021).
27. S. Basu, M. W. Hyde, X. Xiao, D. G. Voelz, and O. Korotkova, "Computational approaches for generating electromagnetic Gaussian Schell-model sources," Opt. Express **22**, 31691 (2014).
28. D. Voelz, X. Xiao, and O. Korotkova, "Numerical modeling of Schell-model beams with arbitrary far-field patterns," Opt. Lett. **40**, 352 (2015).
29. F. Wang, J. Li, G. Martinez-Piedra, and O. Korotkova, "Propagation dynamics of partially coherent crescent-like optical beams in free space and turbulent atmosphere," Opt. Express **25**, 26055 (2017).
30. X. Wang, J. Tang, Y. Wang, X. Liu, C. Liang, L. Zhao, B. J. Hoenders, Y. Cai, and P. Ma, "Complex and phase screen methods for studying arbitrary genuine Schell-model partially coherent pulses in nonlinear media," Opt. Express **30**, 24222 (2022).
31. H. Lajunen, J. Lancis, E. Silvestre, and P. Andrés, "Pulse-by-pulse method to characterize partially coherent pulse propagation in instantaneous nonlinear media," Opt. Express **18**, 14979 (2010).
32. H. Wang, X.-L. Ji, H. Zhang, X.-Q. Li, and Y. Deng, "Propagation formulae and characteristics of partially coherent laser beams in nonlinear media," Opt. Lett. **44**, 743 (2019).
33. H. Wang, X. Ji, Y. Deng, X. Li, and H. Yu, "Theory of the quasi-steady-state self-focusing of partially coherent light pulses in nonlinear media," Opt. Lett. **45**, 710 (2020).
34. L. Lu, Z. Wang, J. Yu, C. Qiao, R. Lin, and Y. Cai, "Self-focusing property of partially coherent beam with non-uniform correlation structure in nonlinear media," Front. Phys. **9**, 728 (2022).
35. F. Gori and M. Santarsiero, "Devising genuine spatial correlation functions," Opt. Lett. **32**, 3531 (2007).
36. F. Gori, V. Ramírez-Sánchez, M. Santarsiero, and T. Shirai, "On genuine cross-spectral density matrices," J. Opt. A Pure Appl. Opt. **11**, 085706 (2009).
37. B. Hermansson, D. Yevick, and A. T. Friberg, "Optical coherence calculations with the split-step fast Fourier transform method," Appl. Opt. **25**, 2645 (1986).
38. D. Jianqin, W. Youwen, Z. Lifu, Z. Jin, and W. Shuangchun, "Transmission characteristics of 1-dimensional intensity modulation of femtosecond pulsed laser," Intense Laser Part. Beam **22**, 1709 (2010).